arXiv:hep-ph/0202238v1 25 Feb 2002

NT@UW–02–003

HIGH ENERGY QCD AND THE LARGE N_C LIMIT

YURI V. KOVCHEGOV
Department of Physics, University of Washington, Box 351560
Seattle, WA 98195
E-mail: yuri@phys.washington.edu

We review recent progress in understanding QCD at high energies and the role played in it by the large N_c limit. We discuss unitarization of total hadronic cross sections and saturation of structure functions at high energies.

1 The BFKL Equation

One of the most important problems in QCD is the problem of understanding its high energy asymptotics. High energy QCD has direct relevance to the scattering data produced at the accelerators worldwide allowing for experimental verification of theoretical attempts to understand QCD dynamics. In addition to that gluonic fields in this extreme regime of high energies become very strong making the underlying description of QCD processes non-perturbative, while leaving the strong coupling constant α_s small. Therefore understanding the gluon dynamics and correct degrees of freedom of QCD at high energies is possible and may shed some light on the non-perturbative dynamics of the theory.

Let us consider a scattering of two heavy quarkonia (quark–antiquark states), or, equivalently, scattering of two virtual photons with large virtualities Q_1^2 and Q_2^2, each of which splits into a quark–antiquark pair. Large virtualities or large masses of the quarkonia insure that the strong coupling constant is small, $\alpha_s(Q_1^2) \sim \alpha_s(Q_2^2) \ll 1$, allowing us to use perturbative expansion.

At the lowest order in α_s the simplest model of high energy interaction between the two quarkonia is given by a two gluon exchange in the forward amplitude. The corresponding total cross section of onium–onium scattering is independent of energy at very high energies and could be written as

$$\sigma \sim s^0, \tag{1}$$

where s is the center of mass energy of the system. This model of high energy interactions is known as Low-Nussinov pomeron.[1] It demonstrates that exchanging two vector particles (gluons) between the onia gives a non-vanishing cross section at high energy, while using scalars or fermions (with

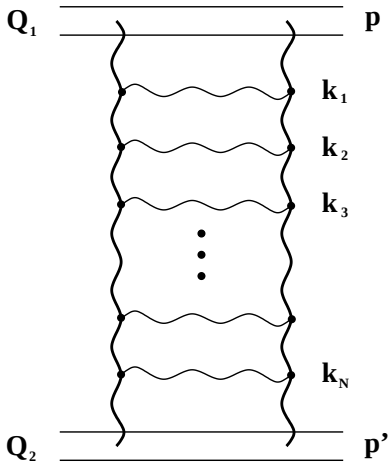

Figure 1. Ladder diagrams summed by the BFKL evolution equation.

non-derivative couplings) would give a cross section that decreases with energy.

However, at the high energies achievable by the modern days accelerators the hadronic cross sections are not constant. They tend to increase as powers of center of mass energy of the system

$$\sigma \sim s^{\Delta} \tag{2}$$

where Δ is a number called pomeron intercept. The rise of partonic structure functions with energy could be described by the DGLAP evolution equation.[2] Nevertheless the DGLAP equation does not yield us with a power of energy growth of the cross sections. The only way to obtain a cross section in perturbative QCD that grows as a power of energy is given by the BFKL evolution equation.[3]

The BFKL equation [3] resums ladder diagrams in the forward onium–onium scattering amplitude of the type shown in Fig. 1. The light cone momenta components of the s-channel gluons are ordered (Regge kinematics) such that

$$p_+ \gg k_{1+} \gg k_{2+} \ldots \gg k_{N+} \gg p'_+ \tag{3}$$

and

$$p_- \ll k_{1-} \ll k_{2-} \ldots \ll k_{N-} \ll p'_- \tag{4}$$

while there is no restrictions on their transverse momenta which remain of the same order throughout the ladder

$$Q_1 \sim k_{1\perp} \sim k_{2\perp} \sim \ldots \sim k_{N\perp} \sim Q_2. \tag{5}$$

Each s-channel gluon in the ladder brings in an extra power of the coupling constant $\alpha_s \ll 1$. The integration over the longitudinal phase space of each gluon gives a term proportional to $\ln s \gg 1$. Combining the two factors we see that each extra s-channel gluon introduces a factor of $\alpha_s \ln s \sim 1$. Thus, by resumming ladders of the type shown in Fig. 1 the BFKL equation resums all powers of the effective parameter $\alpha_s \ln s$.

By drawing a ladder in Fig. 1 we are oversimplifying the problem. The triple gluon vertices in the ladder are not the usual QCD triple gluon vertices. These are the so-called effective Lipatov vertices and have to be calculated by analyzing several gluon emission diagrams[3], though in certain gauges they do correspond to the usual triple gluon vertices. The gluon propagators in the t-channel are also not just the usual gluon propagators. They include virtual (reggeization) corrections to the ladder which modify the gluon propagators. The resulting reggeized gluons are denoted by thick lines in Fig. 1, each line representing a summation of the whole ladder of Fig. 1 in the color octet channel.

The BFKL equation could be written for onium-onium scattering amplitude $f(Q_1, Q_2, Y)$ as [3,4,5]

$$\frac{\partial f(\underline{l}, \underline{l}', Y)}{\partial Y} = \int d^2k \, K_{BFKL}(\underline{l}, \underline{k}) \, f(\underline{k}, \underline{l}', Y) \tag{6}$$

where $Y = \ln(s/Q_1 Q_2)$ is the rapidity variable and K_{BFKL} is the kernel of the equation. Defining the Laplace-transformed amplitude as

$$f_\omega(\underline{l}, \underline{l}') = \int_0^\infty dY \, e^{-\omega Y} \, f(\underline{l}, \underline{l}', Y) \tag{7}$$

Eq. (6) could be rewritten as [3,4,5]

$$\omega f_\omega(\underline{l}, \underline{l}') = \delta^2(\underline{l} - \underline{l}') + \frac{\alpha N_c}{\pi^2} \int \frac{d^2k}{(\underline{k} - \underline{l})^2} \left[f_\omega(\underline{k}, \underline{l}') - \frac{l^2 f_\omega(\underline{l}, \underline{l}')}{k^2 + (\underline{k} - \underline{l})^2} \right]. \tag{8}$$

The solution of Eq. (8) in the saddle point approximation at large Y yields the scattering amplitude

$$f(Q_1, Q_2, Y) = \frac{1}{2\pi Q_1 Q_2 \sqrt{4\pi D Y}} \, e^{(\alpha_P - 1)Y} \, \exp\left[-\frac{\ln^2 Q_1/Q_2}{4\, D\, Y} \right] \tag{9}$$

with $D = \frac{7\alpha_s}{2\pi} N_c \zeta(3)$ and $\alpha_P - 1 = \frac{4\alpha_s N_c}{\pi} \ln 2$. At very high energy the solution given by Eq. (9) grows as a power of energy since

$$e^{(\alpha_P - 1)Y} \sim s^{\alpha_P - 1}. \tag{10}$$

Therefore the BFKL equation seems to be a natural candidate for the phenomenological pomeron as observed in high energy scattering experiments. It is beyond the scope of this talk to address the issue of how well the BFKL equation describes the data. We just note that the numerical value of the obtained pomeron intercept $\alpha_P - 1 = \frac{4\alpha_s N_c}{\pi} \ln 2 \approx 2.6\,\alpha_s \approx 0.8$ is higher than the experimental value of $0.2 - 0.3$ observed in deep inelastic scattering experiments. The inclusion of next-to-leading order correction to BFKL kernel makes the intercept negative for all reasonable values of α_s [6,7,8], though this problem is likely to be due to collinear singularities and should be cured at higher orders in α_s [9] resulting in a slightly lower but still positive value of the intercept which is closer to experimental data. The BFKL equation as described here is applicable only to the scattering of perturbative (small) objects like heavy quarkonia and can not be applied to the total cross section in, say, proton–proton collisions, where (in the single ladder approximation) there is no hard scale which would justify the small coupling approach.

However, the BFKL equation poses some important questions even in the case of heavy onium-onium scattering and at the leading order in α_s in the kernel.

(i) The power of energy growth of the total cross section (Eq. (10)) violates Froissart unitarity bound, which states that the growth of the total cross sections with energy at asymptotically high energies is bounded by [10]

$$\sigma \leq \frac{const}{m_\pi^2} \ln^2 s \tag{11}$$

with m_π the pion's mass. (For a good pedagogical derivation of Froissart bound I refer the readers to [11].) That means some new effects should modify the BFKL equation at very large s to make the resulting amplitude unitary.

(ii) The solution of Eq. (9) includes a diffusion term. To see this let us consider a half of the ladder, from one of the onia to some intermediate gluon in the middle of the ladder carrying momentum $k_\perp$ and rapidity $Y/2$. Applying Eq. (9) to that half-ladder we see that it includes a term

$$\exp\left[-\frac{\ln^2 k_\perp/Q}{2\,D\,Y}\right]. \tag{12}$$

This term is responsible for diffusion of the transverse momenta from the initial perturbative scale Q both into infrared and ultraviolet. The width of

the diffusion grows with rapidity Y. Thus no matter how large the starting scale Q is at certain very high energy the momentum of some gluons in the middle of the ladder would become of the order of Λ_{QCD} invalidating further application of BFKL evolution.[12] Again this hints that the BFKL equation should be modified at higher energies to avoid this problem.

2 Multiple Reggeon Exchanges

The BFKL ladder in Fig. 1 can be viewed as two reggeized gluons (reggeons) propagating in the t-channel. It has been conjectured that unitarity of the total cross section could be restored if one resums all diagrams with multiple reggeon exchanges [13]. Instead of summing the ladder in Fig. 1 one has to analyze all the diagrams of the type shown in Fig. 2. There one can exchange any number of reggeons in the t-channel. Each pair of reggeons may interact via s-channel gluon exchanges leading to BFKL-type contributions. To complete the picture one should also include the diagrams where the number of reggeons varies in the t-channel, that is the diagrams containing vertices of n reggeons going into m reggeons for any n and m. This is beyond the scope of this talk. We are going to concentrate on the diagrams where the number of reggeons is constant.

The n-reggeon exchange diagrams were first resummed by Matinyan and Sedarkyan [14] for the scalar ϕ^3 theory. For n-reggeon exchange amplitude one can write down an equation similar to Eq. (6). However there are many

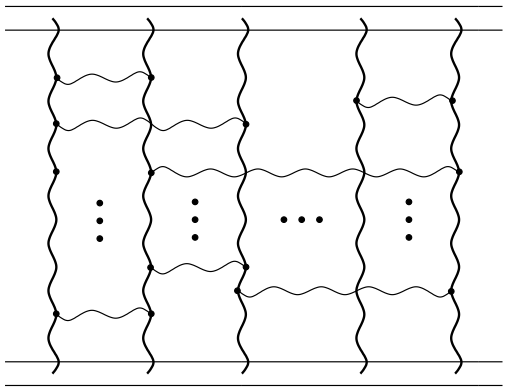

Figure 2. Multiple reggeon exchange diagram.

more contributions to the kernel than in the 2-reggeon case considered above. Since at each step in rapidity any two out of n reggeons can interact one expects $n(n-1)/2$ contributions to the kernel of the integral equation. Each contribution comes in with the same integral kernel acting on a different pair of reggeons. Assuming for simplicity that all these kernels are approximately the same we can write the following equation for n-reggeon amplitude $\mathcal{F}_n$ at large n

$$\frac{\partial \mathcal{F}_n}{\partial Y} \approx n^2 \, K \otimes \mathcal{F}_n. \tag{13}$$

The solution of Eq. (13) scales as

$$\mathcal{F}_n(Y) \sim e^{(-2n+\text{const}\, n^2)Y} \sim s^{-2n+\text{const}\, n^2}, \tag{14}$$

where the term $-2n$ in the power results from the fact that we are dealing with n scalar particles in ϕ^3 theory. The total cross section would be given by the sum of n-reggeon amplitudes

$$\sigma \sim \sum_n \mathcal{F}_n \sim \sum_n c_n \, s^{-2n+\text{const}\, n^2}, \tag{15}$$

which is not likely to converge! (c_n's are some coefficients which may depend on s at most logarithmically.) This result indicates that multiple reggeon exchanges in ϕ^3 theory not only fail to unitarize the total cross section, but rather make the series highly divergent. It is believed that the problem is associated to the fact that ϕ^3 theory has no stable vacuum and is typical only to ϕ^3 theory. Nevertheless one might and should get worried about similar phenomenon happening in QCD.

To demonstrate that the catastrophe which happened in ϕ^3 theory is actually avoided in QCD one has to invoke the 't Hooft large N_c limit [15] which is the central topic of this conference. In the large N_c limit the diagrams in Fig. 2 drastically simplify: only the planar graphs survive. Thus the topology of the interaction takes form of a cylinder with the reggeons forming the walls of the cylinder and only the interactions of the nearest neighbor reggeons are allowed, as depicted in Fig. 3. There the ith reggeon may interact only with the $i-1$st and $i+1$st reggeons, and the 1st reggeon interacts with the nth and the 2nd reggeons. The two reggeon case (the pomeron of Fig. 1) corresponds to the simplest cylinder topology case with reggeons and s-channel gluons "living" on the walls of a cylinder. If we add one more reggeon we would obtain the three reggeon case (odderon) which also has a cylindrical topology as shown in Fig. 3.

With only the nearest neighbor interactions between the reggeons allowed the kernel of the integral equation resumming the diagrams shown in Fig. 3

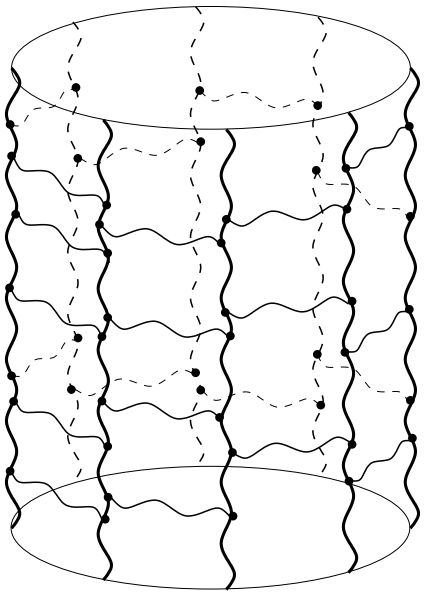

Figure 3. An example of cylinder topology acquired by multiple reggeon exchange diagrams in the large N_c limit. The ellipses are drawn to guide the eye.

receives only n contributions, which is very different from ϕ^3 theory. Making the same assumption as for ϕ^3 theory we see that Eq. (13) for large-N_c QCD becomes

$$\frac{\partial \mathcal{F}_n}{\partial Y} \approx n\, K \otimes \mathcal{F}_n \tag{16}$$

leading to

$$\mathcal{F}_n(Y) \sim e^{\text{const}\, n\, Y} \sim s^{\text{const}\, n}. \tag{17}$$

Now the total cross section similar to Eq. (15) is

$$\sigma \sim \sum_n \mathcal{F}_n \sim \sum_n d_n\, s^{\text{const}\, n}, \tag{18}$$

with d_n's some coefficients with weak dependence on s. The series in Eq. (18) could be convergent and therefore large-N_c QCD avoids the catastrophe of ϕ^3 theory. One expects that the problem would not reappear for the real life case

of three colors. We have to advise the reader to understand Eq. (17) only as an upper bound on the n reggeon amplitudes but not as an exact answer.

A careful QCD analysis of the reggeon cylinder graphs of the type shown in Fig. 3 demonstrates that a reggeon system is equivalent to a one dimensional XXX Heisenberg spin chain for spin $S = 0$ and is thus an exactly solvable model [17]. That facilitates the analysis of the n-reggeon diagrams allowing to quantitatively understand their high energy behavior.[18]

An important question for the total cross section is whether the leading-N_c $2n$-reggeon diagram gives an amplitude which grows with energy faster than the subleading in N_c n-pomeron diagram. Naturally the n-pomeron diagram should scale as $s^{n(\alpha_P-1)}$. In the recent paper by Korchemsky et al[18] it has been shown that the n reggeon amplitude seem to scale as $\mathcal{F}_n \sim s^{\text{const}/n}$. Thus at very high energies multiple reggeon exchange diagrams grow much slower than multiple pomeron exchange diagrams and the former could be neglected compared to the latter. We refer the interested readers to the contribution of G. Korchemsky in these proceedings [18].

3 Multiple Pomeron Exchanges

3.1 General Physical Picture

As could be seen from the discussion in the previous section an exchange of a single BFKL pomeron brings in a parametrical factor of $\alpha_s^2\, e^{(\alpha_P-1)Y}$, where $e^{(\alpha_P-1)Y}$ comes from the amplitude in Eq. (9) and the factor of α_s^2 comes from connecting the reggeons in the ladder to the onia. The BFKL equation resums powers of $(\alpha_P - 1)Y \sim \alpha_s Y$ and therefore gives a large contribution when

$$Y_{LO} \sim \frac{1}{\alpha_s}. \tag{19}$$

What happens as we increase the energy/rapidity? It is possible that multiple pomeron exchanges would start playing a bigger role in the scattering. To estimate when this happens we have to equate single $(\alpha_s^2\, e^{(\alpha_P-1)Y})$ and double $(\alpha_s^4\, e^{2(\alpha_P-1)Y})$ pomeron contributions, effectively requiring that $\alpha_s^2\, e^{(\alpha_P-1)Y_U} \sim 1$. As was argued by Mueller in [19] multiple pomeron exchanges become important at the values of rapidity of the order of

$$Y_U \sim \frac{1}{\alpha_P - 1}\, \ln \frac{1}{\alpha_s^2}. \tag{20}$$

After completion of the calculation of the next–to–leading order corrections to the kernel of the BFKL equation (NLO BFKL) by Fadin and Lipatov

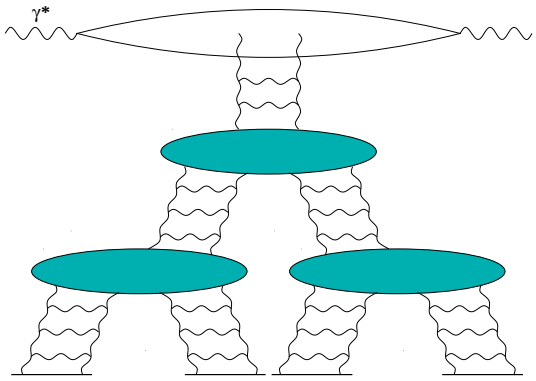

Figure 4. An example of the pomeron "fan" diagram. Each ladder interacts with the proton or nucleus at rest independently.

[6], and, independently, by Camici and Ciafaloni [7], it was shown in [8] that due to the running coupling effects these corrections become important at the rapidities of the order of

$$Y_{NLO} \sim \frac{1}{\alpha_s^{5/3}}. \tag{21}$$

One can see that $Y_{LO} \ll Y_U \ll Y_{NLO}$ for parametrically small α_s. That implies that the center of mass energy at which the multiple pomeron exchanges become important is much smaller, and, therefore, is easier to achieve, than the energy at which NLO corrections start playing an important role. That is multiple pomeron exchanges are probably more relevant than NLO BFKL to the description of current experiments.[20] Also multiple pomeron exchanges are much more likely to unitarize the total hadronic cross section. Here we are going to present a solution to the problem of resummation of multiple pomeron exchanges and show how the BFKL pomeron unitarizes following[21].

We will consider deep inelastic scattering (DIS) of a virtual photon on a hadron or nucleus and will resum all multiple pomeron exchanges contributing to the total DIS cross section in the leading longitudinal logarithmic approximation in the large N_c limit. The first step in that direction in perturbative QCD was a conjecture by Gribov, Levin and Ryskin (GLR)[22] of an equation describing the fusion of two pomeron ladders into one, which was proven in the double logarithmic limit by Mueller and Qiu.[23] The resulting equation resums all pomeron "fan" diagrams (see Fig. 4) in the double logarithmic approximation. An extensive work on resumming the multiple pomeron exchanges in the

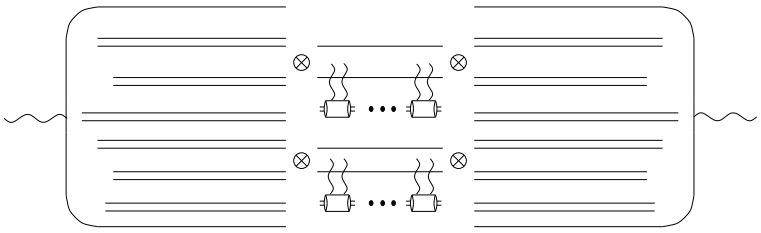

Figure 5. Dipole evolution in the deep inelastic scattering process as pictured in[21]. The incoming virtual photon develops a system of color dipoles, each of which rescatters on the target hadron or nucleus (only two are shown).

gluon distribution function in the leading $\ln(1/x)$ approximation (i.e. without taking the double logarithmic limit) both in the framework of effective field theories and employing alternative approaches has been pursued in [24,25,26,27].

Let us consider a deep inelastic scattering (DIS) of a virtual photon on a hadron or nucleus. An incoming photon splits into a quark–antiquark pair and then the $q\overline{q}$ pair rescatters on the target hadron or nucleus. In the rest frame of the hadron all QCD evolution should be included in the wave function of the incoming photon. That way the incoming photon develops a cascade of gluons, which then scatter on the hadron at rest. We want to calculate this gluon cascade in the leading longitudinal logarithmic $(\ln 1/x)$ approximation and in the large N_c limit. This is exactly the type of cascade described by Mueller's dipole model[28]. In the large N_c limit the incoming gluon develops a system of color dipoles and each of them independently rescatters on the hadron or nucleus. The forward amplitude of the process is shown in Fig. 5. The double lines in Fig. 5 correspond to gluons in large N_c approximation being represented as consisting of a quark and an antiquark of different colors. The color dipoles are formed by a quark from one gluon and an antiquark from another gluon. In Fig. 5 each dipole, that was developed through the QCD evolution, later interacts with the hadron or nucleus by a series of Glauber–type multiple rescatterings on the sources of color charge. The assumption about the type of interaction of the dipoles with the hadron is not important for the evolution. It could also be just two gluon exchanges. The important assumption is that each dipole interacts with the target independently of the other dipoles, which is done in the spirit of the large N_c limit and is valid for a model of a large dilute target nucleus.

For the case of a dilute target independent dipole interactions with the target proton or nucleus are enhanced by some factors of the number of

sources of color charge in the proton or nucleus compared to the case when several dipoles interact with the same parton in the proton or the same nucleon in the nucleus.[29,30] This allowed us to assume that the dipoles interact with the proton or nucleus independently. In case of a nucleus one actually has the atomic number A as a parameter leading powers in which justify this approximation.[29,30] The summation of these contributions corresponds to summation of the pomeron "fan" diagrams of Fig. 4. In general there is another class of diagrams, which we will call pomeron loop diagrams. In a pomeron loop diagram a pomeron first splits into two pomerons, just like in the fan diagram, but then the two pomerons merge back into one pomeron. The graphs containing pomerons not only splitting, but also merging together will be referred to as pomeron loop diagrams. In a dilute proton or nucleus these pomeron loop diagrams could be considered small, since they would be suppressed by powers of color charge density (A). At very high energies this approximation becomes not very well justified even in the dilute target case. Contribution of each additional pomeron in a fan diagram on a hadron is parametrically of the order of $\alpha_s^2 A^{1/3} e^{(\alpha_P - 1)Y}$ which is large at the rapidities of the order of Y_U given by Eq. (20). The contribution of an extra pomeron in a pomeron loop diagram is of the order of $\alpha_s^2 e^{(\alpha_P - 1)Y}$, which is not enhanced by powers of A and is, therefore, suppressed in the dilute nucleus case. However, one can easily see that at extremely high energies, when $\alpha_s^2 e^{(\alpha_P - 1)Y}$ becomes greater than one, pomeron loop diagrams become important, still being smaller than the fan diagrams. Resummation of pomeron loop diagrams in a dipole wave function seems to be a very hard technical problem, possibly involving NLO BFKL or, even, next-to-next-to-leading order BFKL kernel calculations.[31] Nevertheless, it is the author's belief that while being crucial for onium–onium scattering the pomeron loop diagrams are not going to significantly change the high energy behavior of the DIS structure functions.

3.2 Nonlinear Evolution Equation

We start by considering a deep inelastic scattering process. The incoming virtual photon with a large q_+ component of the momentum splits into a quark–antiquark pair which then interacts with the target at rest. We model the interaction by no more than two gluon exchanges between each source of color charge and the quark–antiquark pair. This is done in the spirit of the quasi–classical approximation used previously in [32,33]. The interactions are taken in the eikonal approximation. Then, as could be shown in general, i.e., including the leading logarithmic QCD evolution, the total cross–section, and, therefore, the F_2 structure function of the nucleus can be rewritten as a

product of the square of the virtual photon's wave function and the propagator of the quark–antiquark pair through the proton. The expression reads

$$F_2(x,Q^2) = \frac{Q^2}{4\pi^2\alpha_{EM}} \int \frac{d^2\mathbf{x}_{01}dz}{2\pi} \left[\Phi_T(\mathbf{x}_{01},z)+\Phi_L(\mathbf{x}_{01},z)\right] d^2b_0 \; N(\mathbf{x}_{01},\mathbf{b}_0,Y), \tag{22}$$

where the incoming photon with virtuality Q splits into a quark–antiquark pair with the transverse coordinates of the quark and antiquark being $\tilde{\mathbf{x}}_0$ and $\tilde{\mathbf{x}}_1$ correspondingly, such that $\mathbf{x}_{10} = \tilde{\mathbf{x}}_1 - \tilde{\mathbf{x}}_0$. The coordinate of the center of the pair is given by $\mathbf{b}_0 = \frac{1}{2}(\tilde{\mathbf{x}}_1 + \tilde{\mathbf{x}}_0)$. The square of the light cone wave function of $q\overline{q}$ fluctuations of a virtual photon is denoted by $\Phi_T(\mathbf{x}_{01},z)$ and $\Phi_L(\mathbf{x}_{01},z)$ for transverse and longitudinal photons correspondingly, with z being the fraction of the photon's longitudinal momentum carried by the quark. $\Phi_T(\mathbf{x}_{01},z)$ and $\Phi_L(\mathbf{x}_{01},z)$ are known functions and could be found in the literature.[34]

The quantity $N(\mathbf{x}_{01},\mathbf{b}_0,Y)$ has the meaning of the forward scattering amplitude of the quark–antiquark pair on a nucleus. At the lowest (classical) order not including the QCD evolution in rapidity it is given by

$$N(\mathbf{x}_{01},\mathbf{b}_0,0) = -\gamma(\mathbf{x}_{01},\mathbf{b}_0) \approx \left\{1 - \exp\left[-\frac{\alpha_s\pi^2}{2N_cS_\perp}\mathbf{x}_{01}^2 A\, xG(x,1/\mathbf{x}_{01}^2)\right]\right\}. \tag{23}$$

$\gamma(\mathbf{x}_{01},\mathbf{b}_0)$ is the propagator of the $q\overline{q}$ pair through the hadron or nucleus. The propagator could be easily calculated, similarly to [32,33], giving the Glauber multiple rescattering formula (23). Throughout the talk we assume for simplicity that the target nucleus is a cylinder, which appears as a circle of radius R in the transverse direction and has a constant length $2R$ along the longitudinal z direction. Therefore its transverse cross–sectional area is $S_\perp = \pi R^2$. In formula (23) α_s is the strong coupling constant and $xG(x,1/\mathbf{x}_{01}^2)$ is the gluon distribution of a nucleon in the nucleus, taken at the lowest order in α_s, similarly to [33].

Eq. (23) resums all Glauber type multiple rescatterings of a $q\overline{q}$ pair on a target nucleus. As was mentioned before, since each interaction of the pair with a source of color charge in the nucleus is restricted to the two gluon exchange, the formula (23) effectively sums up all the powers of the parameter $\alpha_s^2A^{1/3}$. (Since $xG \sim C_F$ there is no N_c present in the expansion in the large-N_c limit.) Therefore this interaction of course is subleading in N_c as is true for any hadronic interactions.[15]

Since the target is at rest in order to include the QCD evolution of F_2 structure function, we have to develop the soft gluon wave function of the incoming virtual photon. In the leading longitudinal logarithmic approxima-

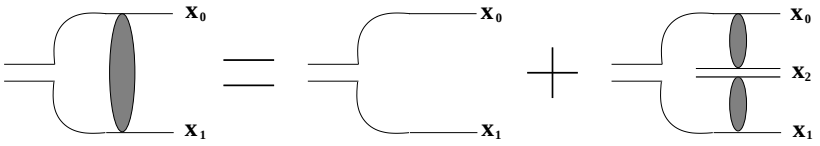

Figure 6. A diagrammatic representation of the dipole evolution equation.

tion ($\ln 1/x$) the evolution of the wave function is realized through successive emissions of small–x gluons. The $q\overline{q}$ pair develops a cascade of gluons, which then scatter on the hadron. In order to describe the soft gluon cascade we will take the limit of a large number of colors, $N_c \to \infty$. Then, this leading logarithmic soft gluon wavefunction will become equivalent to the dipole wave function, introduced by Mueller in [28]. The physical picture becomes straightforward. The $q\overline{q}$ pair develops a system of dipoles (dipole wave function), and each of the dipoles independently scatters on the target hadron or nucleus (see Fig. 5). Since the target is assumed to have many sources of color charge in it we may approximate the interaction of a dipole (quark–antiquark pair) with it by $\gamma(\mathbf{x}, \mathbf{b})$ given by Eq. (23), with $\mathbf{x}$ and $\mathbf{b}$ being the dipole's transverse separation and impact parameter. That means that each of the dipoles interacts with several sources of color charge (Glauber rescattering) in the nucleus independent of other dipoles.

To construct the dipole wave function we will heavily rely on the techniques developed in [28]. We have to resum a gluonic cascade in the large-N_c limit. Denoting the cascade by a blob we can write down an equation which is illustrated in Fig. 6. As usual for the large N_c limit the double line denotes a gluon. The original $q\bar{q}$ pair may have no evolution in it, i.e., the cascade could be empty, as illustrated by the first term on the right hand side of Fig. 6. In one step of the evolution in rapidity a gluon is emitted in a dipole, splitting the parent dipole into two dipoles. Each of the produced dipoles is nonlocal: it consists of a quark (antiquark) from the original quark–antiquark pair and an antiquark (quark) component of the emitted gluon. The consecutive gluon evolution can continue in either of the two dipoles. This is depicted in the second term on the right hand side of Fig. 6. This procedure gives us a self-consistent equation resumming the gluon cascade.[28,21]

Substituting $1 - N(\mathbf{x}_{01}, \mathbf{b}_0, Y)$ instead of the blob symbolizing the gluon cascade and including virtual corrections one obtains the following equation[21]

$$N(\mathbf{x}_{01}, \mathbf{b}_0, Y) = -\gamma(\mathbf{x}_{01}, \mathbf{b}_0) \, \exp\left[-\frac{4\alpha_s C_F}{\pi} \ln\left(\frac{x_{01}}{\rho}\right) Y\right]$$

$$+\frac{\alpha_s C_F}{\pi^2}\int_0^Y dy\,\exp\left[-\frac{4\alpha_s C_F}{\pi}\ln\left(\frac{x_{01}}{\rho}\right)(Y-y)\right]$$

$$\times\int_\rho d^2\tilde{x}_2\frac{x_{01}^2}{x_{02}^2x_{12}^2}\,[2\,N(\mathbf{x}_{02},\mathbf{b}_0+\frac{1}{2}\mathbf{x}_{12},y)$$

$$-N(\mathbf{x}_{02},\mathbf{b}_0+\frac{1}{2}\mathbf{x}_{12},y)\,N(\mathbf{x}_{12},\mathbf{b}_0-\frac{1}{2}\mathbf{x}_{20},y)]. \tag{24}$$

Equation (24), together with Eq. (22), provide us with the leading logarithmic evolution of the F_2 structure function of a hadron including all multiple pomeron exchanges in the large–N_c limit. Note that while the evolution is leading in N_c the interactions (γ) are not, so that Eq. (24) could be viewed as resumming powers of $\alpha_s^2 A^{1/3}\,e^{\alpha_s N_c Y}$.

Similar evolution equation was obtained by Balitsky in [26] using an effective lagrangian approach to high energy QCD. The evolution equations obtained in [26] reduce to a closed single equation only in the large-N_c limit. Similar results have been obtained in [24,25].

3.3 Solution of the Nonlinear Evolution Equation

To understand the qualitative features of the integral equation (24) it is convenient to rewrite it in the differential form. Assuming that the typical size of the dipole wave function $x_\perp \ll R$, where R is the proton's radius, we can rewrite Eq. (24) as

$$\frac{\partial N(\mathbf{x}_{01},Y)}{\partial Y}=\frac{2\alpha_s C_F}{\pi^2}\int_\rho d^2x_2\left[\frac{x_{01}^2}{x_{02}^2x_{12}^2}-2\pi\delta^2(\mathbf{x}_{01}-\mathbf{x}_{02})\ln\left(\frac{x_{01}}{\rho}\right)\right]N(\mathbf{x}_{02},Y)$$

$$-\frac{\alpha_s C_F}{\pi^2}\int d^2x_2\,\frac{x_{01}^2}{x_{02}^2x_{12}^2}\,N(\mathbf{x}_{02},Y)\,N(\mathbf{x}_{12},Y). \tag{25}$$

Performing a Fourier transform

$$N(x_\perp,Y)=x_\perp^2\int\frac{d^2k}{2\pi}\,e^{i\mathbf{k}\cdot\mathbf{x}}\,\tilde{N}(k,Y)=x_\perp^2\int_0^\infty dk\,k\,J_0(kx_\perp)\,\tilde{N}(k,Y). \tag{26}$$

we obtain

$$\frac{\partial\tilde{N}(k,Y)}{\partial Y}=\frac{2\alpha_s N_c}{\pi}\,\chi\left(-\frac{\partial}{\partial\ln k}\right)\,\tilde{N}(k,Y)-\frac{\alpha_s N_c}{\pi}\,\tilde{N}^2(k,Y), \tag{27}$$

where

$$\chi(\lambda)=\psi(1)-\frac{1}{2}\psi\left(1-\frac{\lambda}{2}\right)-\frac{1}{2}\psi\left(\frac{\lambda}{2}\right) \tag{28}$$

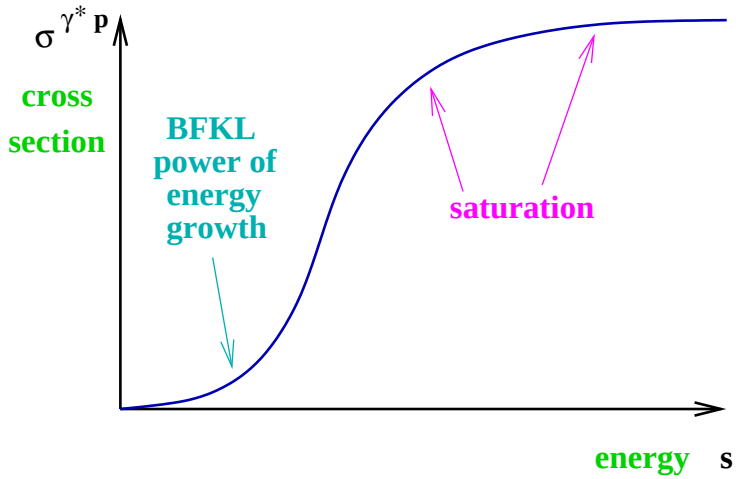

Figure 7. Qualitative behavior of the total DIS cross section given by the solution of Eq. (24).

is the eigenvalue of the BFKL kernel [3] with $\psi(\lambda) = \Gamma'(\lambda)/\Gamma(\lambda)$. In Eq. (27) the function $\chi(\lambda)$ is taken as a differential operator with $\lambda = -\partial/\partial \ln k$ acting on $\tilde{N}(k, Y)$. We also put $N_c/2$ instead of C_F everywhere in the spirit of the large N_c approximation. The details of obtaining Eq. (27) from Eq. (25) could be found in [21].

Now the physical meaning of the evolution given by Eq. (24) becomes manifest. The linear part of Eq. (27) is just the familiar BFKL equation, giving a cross section growing as a power of energy. When energy is not too large and N is small the quadratic term could be neglected and the linear evolution is all that remains. However as the energy increases the evolution driven by BFKL would make N large, making the quadratic term in Eq. (27) important. The quadratic term would introduce damping effects, similar to GLR-MQ equation[22,23], slowing down the growth of the cross section and possibly unitarizing it.

Eq. (24) has been solved both analytically by approximate methods [21,35] and numerically[35,36,37,38]. The result for DIS cross sections is qualitatively illustrated in Fig. 7. The cross section starts growing as a power of energy and then saturates to a much slower (logarithmic) growth.[21,35] Thus Eq. (24) resolves the problem of unitarization of BFKL pomeron **(i)** posed in Sect. 1.

Does Eq. (24) answer the second question **(ii)** posed in Sect. 1? Let us first note that Eq. (24) produces a large momentum scale which grows with energy as predicted within the framework of McLerran-Venugopalan model[29,24,25]. To see this let us write down the solution to Eq. (27) in the limit of moderate energies (where the equation is still mostly linear):

$$\tilde{N}_1(k,Y) = C\,\frac{\Lambda}{k}\,\frac{\exp[(\alpha_P-1)Y]}{\sqrt{14\alpha_s N_c\zeta(3)Y}}\exp\left(-\frac{\pi}{14\alpha_s N_c\zeta(3)Y}\ln^2\frac{k}{\Lambda}\right), \qquad (29)$$

where C is some overall normalization constant and Λ is the momentum scale inherent to the initial distribution given by Eq. (23) (in fact it is the classical saturation scale given by McLerran-Venugopalan model[29,30,33]). At very high energy the amplitude N saturates to a constant: $N \to 1$ as $Y \to \infty$. In momentum space this corresponds to[21]

$$\tilde{N}_{sat}(k,Y) = \ln\frac{Q_s}{k}. \qquad (30)$$

Logarithm is a slowly varying function compared to exponent and to estimate at what momentum scale the transition to saturation takes place we can just equate the amplitude in Eq. (29) to one. Omitting all slowly varying with Y prefactors we obtain an estimate of the the saturation scale

$$Q_s(Y) \approx \Lambda\,\frac{\exp[(\alpha_P-1)Y]}{\sqrt{14\alpha_s N_c\zeta(3)Y}}. \qquad (31)$$

One can see from Eq. (31) that as energy increases the saturation scale increases too.

Numerical simulation[36,37,38] demonstrated a very interesting behavior of the solution of Eq. (24), which is drastically different from the solution of BFKL. Let us remind the readers that in Sect. 1 based on Eq. (12) we observed that with increasing energy the momentum of gluons given by the solution to BFKL equation diffuses around some initial external perturbative scale Q with the diffusion width increasing with Y. That was potentially dangerous since the diffusion cone would eventually get into the non-perturbative region. The solution of Eq. (24) produces a very different distribution of transverse momenta of the gluons: the width of the diffusion cone seems to be independent of energy while the center of the distribution is given by the saturation scale $Q_s(Y)$ which increases with Y[36,37,38] (see Eq. (31)). Thus the distribution never gets into the dangerous infrared region. Therefore Eq. (24) appears to solve the problem **(ii)** posed in Sect. 1 of the sensitivity of the cross sections given by BFKL evolution to the non-perturbative infrared region.[12]

4 "Phase Diagram" of High Energy QCD

To summarize the results of the previous Section we present the "phase diagram" of high energy QCD depicted in Fig. 8.

The majority of the HERA data shows that the proton's structure functions at large photon's virtuality Q^2 and not very small Bjorken $x \approx Q^2/s$ can be described by the DGLAP evolution equation [2], which is a linear equation. It is convenient to present different properties of hadronic structure functions in terms of a "phase diagram" in Q^2 and $\ln 1/x$ plane (see Fig. 8). The DGLAP physics corresponds to the lower right section of the plane, where Q^2 is large and x is not too small. As one goes towards smaller x in the same region of Q^2 the hadronic structure functions rise. Most of the data in that region can be explained in terms of either small-x limit of DGLAP equation or, alternatively and more interestingly, by the BFKL equation[3], which is also a linear equation but could be responsible for evolving the system towards a higher gluonic density regime. However, the DIS cross sections can not rise forever as powers of center of mass energy s. This would violate unitarity[10] and pose other problems discussed in Sect. 1. That means that at some very small x the hadronic structure functions have to undergo a significant qualitative change of behavior, becoming a much slower varying functions of x. The slow down of the growth of hadronic structure functions is usually associated with non-linear effects in the quark and gluon dynamics, such as parton recombination, which eventually balances the parton splitting process

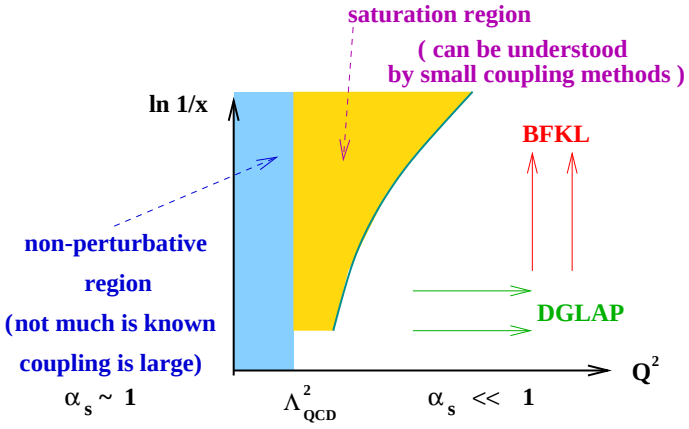

Figure 8. "Phase diagram" of high energy QCD.

as we have seen in the previous Section. The partons in the hadronic wave function reach the state of *saturation*. The region of saturation of the structure functions is represented in yellow in Fig. 8. The scale Q^2 corresponding to the transition to the saturation region is different for different values of Bjorken x, increasing with decreasing x (increasing energy s). This scale is the *saturation scale* $Q_s^2(Y = \ln 1/x)$ given by Eq. (31). If $Q_s^2(x) \gg \Lambda_{QCD}^2$ than the coupling constant inside the saturation region would still be small allowing us to perform analytical calculations inside of the saturation region[29] by employing Eq. (24).

It is possible that the recent experimental data obtained at HERA [20] contains evidence of saturation transition in DIS on a proton at $x \approx 10^{-3} - 10^{-4}$ and $Q^2 \approx 2 - 4\,GeV^2$, providing an experimental confirmation of the theoretical ideas presented above.

5 Open Questions

Several question are still open in the field of saturation physics. Here are some of the questions related to total cross sections:

1. The large N_c limit was instrumental in deriving Eq. (24)[21]. Beyond it the systems of evolution equations in the existing approaches do not seem to close.[26,24,25] Thus the question remains: can one describe the high energy asymptotics of QCD beyond the large-N_c limit?

2. NLO BFKL corrections[6,7] seem to be very large and negative, posing several open questions for the linear evolution equation.[8,9] Would these problems be cured if one calculates the NLO correction to the full nonlinear evolution? Nonlinear effects become important before the NLO effects and may modify the NLO corrections. Work on this project is under way.[39]

3. Finally in this talk we have demonstrated how unitarization happens in DIS cross sections via summation of fan diagrams of Fig. 4. This mechanism would not work for onium-onium scattering cross section, even though a large Q_s should exist in the problem. One has to resum the pomeron loop diagrams[28,31] in order to understand the unitarization of onium–onium cross section (and, correspondingly, the proton-proton cross section). Resummation of pomeron loops is still an important open question in high energy physics.

Acknowledgements

I thank the organizers of *The Phenomenology of Large N_c QCD* workshop for such an interesting and timely meeting. This work has been supported in part by the U.S. Department of Energy under Grant No. DE-FG03-97ER41014 and

by the BSF grant # 9800276 with Israeli Science Foundation, founded by the Israeli Academy of Science and Humanities.

References

1. F.E. Low, Phys. Rev. D **12**, 163 (1975); S. Nussinov, Phys. Rev. Lett. **34**, 1286 (1975).
2. V.N. Gribov and L.N. Lipatov, Sov. J. Nucl. Phys. **15**, 438 (1972); G. Altarelli and G. Parisi, Nucl. Phys. **B 126**, 298 (1977); Yu.L. Dokshitzer, Sov. Phys. JETP **46**, 641 (1977).
3. E.A. Kuraev, L.N. Lipatov and V.S. Fadin, Sov. Phys. JETP **45**, 199 (1977); I.I. Balitsky and L.N. Lipatov, Sov. J. Nucl. Phys. **28**, 822 (1978).
4. A.H. Mueller, *Deep inelastic scattering and small-x physics*, Lectures given at NATO Advanced Study Institute: Frontiers in Particle Physics, Cargese, France, 1-13 Aug 1994, Cargese Summer Inst. **0087-114**, (1994).
5. T. Jaroszewicz, Acta Phys. Polon., **B11**, 965 (1980).
6. V.S. Fadin and L.N. Lipatov, Phys. Lett. B **429**, 127 (1998).
7. M. Ciafaloni and G. Camici, Phys. Lett. B **430**, 349 (1998).
8. Yu. V. Kovchegov, A. H. Mueller, Phys. Lett. B **439**, 428 (1998); E. Levin, hep-ph/9806228.
9. M. Ciafaloni, D. Colferai, Phys. Lett. B **452**, 372 (1999); M. Ciafaloni, D. Colferai, G.P. Salam, Phys. Rev. D **60**, 114036 (1999).
10. M. Froissart, Phys. Rev. **123**, 1053 (1961).
11. E. Levin, hep-ph/9710546.
12. J. Bartels, J. Phys. **G19**, 1611 (1993); J. Bartels, H. Lotter, M. Vogt, Phys. Lett. **B373**, 215 (1996).
13. J. Bartels, *Nucl. Phys.* B**175**, 365 (1980); H. Cheng, J. Dickinson, C. Y. Lo, K. Olaussen, *Phys. Rev.* D**23**, 354 (1981).
14. S. G. Matinyan, A. G. Sedarkyan, Sov. J. Nucl. Phys. **24**, 440 (1976); JETP Lett. **23**, 588 (1976).
15. G. 't Hooft, Nucl. Phys. **B72**, 461 (1974).
16. L.N. Lipatov, *Phys. Lett.* B**251**, 284 (1990); **B309**, 394 (1993); G. Veneziano, *Nucl. Phys.* B**74**, 365 (1974); *Phys. Lett.* B**52**, 220 (1974); A. Schwimmer, G. Veneziano, *Nucl. Phys.* B**81**, 445 (1974); M. Ciafaloni, G. Marchesini, G. Veneziano, *Nucl. Phys.* B**98**, 472 (1975).
17. L.N. Lipatov, JETP Lett **59**, 596 (1994); L. D. Faddeev, G. P. Korchemsky, Phys. Lett. **B342**, 311 (1995).
18. G.P. Korchemsky, J. Kotanski, A.N. Manashov, hep-ph/0111185; G.P.

Korchemsky, these proceedings.
19. A.H. Mueller, Phys. Lett. **B 396**, 251 (1997).
20. ZEUS Coll., J. Breitweg et al., Eur. Phys. J. **C 7**, 609 (1999).
21. Y.V. Kovchegov, Phys. Rev. **D 60**, 034008 (2000); **D 61**, 074018 (2000).
22. L.V. Gribov, E.M. Levin and M.G. Ryskin, Phys. Rept. **100**, 1 (1983).
23. A.H. Mueller and J. Qiu, Nucl. Phys. **B 268**, 427 (1986).
24. J. Jalilian-Marian, A. Kovner, A. Leonidov, and H. Weigert, Nucl. Phys. **B 504**, 415 (1997); Phys. Rev. **D 59**, 014014 (1999); Phys. Rev. **D 59**, 034007 (1999); J. Jalilian-Marian, A. Kovner, and H. Weigert, Phys. Rev. **D 59**, 014015 (1999); A. Kovner, J. G. Milhano, and H. Weigert, Phys. Rev. **D 62**, 114005 (2000).
25. E. Iancu, A. Leonidov and L. McLerran, Nucl. Phys. **A692**, 583 (2001); E. Ferreiro, E. Iancu, A. Leonidov, L. McLerran, hep-ph/0109115.
26. I. Balitsky, Nucl. Phys. **B 463**, 99 (1996); Phys. Rev. D **60**, 014020 (1999); hep-ph/9706411.
27. A.L. Ayala, M.B. Gay Ducati, and E.M. Levin, Nucl. Phys. **B493**, 305 (1997); **B511**, 355 (1998).
28. A.H. Mueller, Nucl. Phys. **B 415**, 373 (1994); A.H. Mueller and B. Patel, Nucl. Phys. **B 425**, 471 (1994); A.H. Mueller, Nucl. Phys. **B 437**, 107 (1995); Z. Chen and A. H. Mueller, Nucl. Phys. **B451**, 579 (1995).
29. L. McLerran and R. Venugopalan, Phys. Rev. **D 49**, 2233 (1994); 3352 (1994); Phys. Rev. **D 50**, 2225 (1994).
30. Yu.V. Kovchegov, Phys. Rev. D **54**, 5463 (1996); **55**, 5445 (1997).
31. Yu. V. Kovchegov, A. H. Mueller and S. Wallon, Nucl. Phys. **B507**, 367 (1997); H. Navelet, R. Peschanski, hep-ph/0201285.
32. A.H. Mueller, Nucl. Phys. **B 335**, 115 (1990).
33. Yu. V. Kovchegov and A. H. Mueller, Nucl. Phys. **B 529**, 451 (1998); Yu. V. Kovchegov, Phys. Rev. D **64**, 114016 (2001); Nucl. Phys. **A692**, 557 (2001); **A698**, 619 (2002); Yu. V. Kovchegov, K. Tuchin, hep-ph/0111362.
34. N.N. Nikolaev, B.G. Zakharov, Z. Phys. **C 49**, 607 (1991).
35. E. Levin and K. Tuchin, Nucl. Phys. **B573**, 833 (2000); Nucl. Phys. **A691**, 779 (2001); Nucl. Phys. **A693**, 787 (2001).
36. M. A. Braun, Eur. Phys. J. C **16**, 337 (2000); hep-ph/0010041; hep-ph/0101070.
37. E. Levin and M. Lublinsky, hep-ph/0104108; M. Lublinsky,E. Gotsman, E. Levin and U. Maor, hep-ph/0102321.
38. K. Golec-Biernat, L. Motyka, A.M. Stasto, hep-ph/0110325.
39. I.I. Balitsky, A.V. Belitsky, hep-ph/0110158.